J Mater Sci: Mater Med (2011) 22:671–682
DOI 10.1007/s10856-011-4245-3

Surface properties and cell adhesion onto allylamine-plasma and amine-plasma coated glass coverslips

Marianne Crespin · Nicolas Moreau · Bernard Masereel · Olivier Feron · Bernard Gallez · Thierry Vander Borght · Carine Michiels · Stephane Lucas

Received: 21 September 2010 / Accepted: 18 January 2011 / Published online: 3 February 2011

Abstract Surface properties of nanoparticles to be used for radioimmunotherapy need to be optimized to allow antibody conjugation while ensuring biocompatibility. We aimed to investigate cell adhesion and proliferation onto different coatings to be used for nanoparticles. C, CH_x or SiO_x coatings deposited onto glass coverslips by magnetron deposition as well as nitrogen functionalized materials synthetized using different reactive sputtering conditions and PPAA (plasma polymerized allylamine) coating, were compared. Amine functionalization did increase hydrophilicity in all the materials tested. Biocompatibility was assessed by measuring cell viability, morphology, attachment, spreading, and pro-inflammatory cytokine secretion. The results show that C and CN_x were the most biocompatible substrates while SiO_x and SiO_xN_y were the most toxic materials. PPAA coatings displayed unexpectedly an intermediate biocompatibility. A correlation could be observed between wettability and cell proliferation except for C coated surface, indicating that more complex processes than hydrophilicity alone are taking place that affect cell functions.

1 Introduction

Lung cancer is the leading cause of cancer-related mortality worldwide in both men and women [1, 2]. Non-small cell lung cancer (NSCLC) accounts for approximately 85% of all lung cancers and its 5-year survival is only 5% [3, 4]. The conventional treatment of extended NSCLC disease combining systemic chemotherapy with sometimes radiotherapy is unfortunately only palliative: it aims to reduce symptoms, to improve life quality, and to prolong patient survival (6–10 weeks) [1]. Therefore, in order to counter this disease, there is a growing demand for more effective new therapeutic strategies. One of them consists of targeting the vasculature that feeds the tumor by radioimmunotherapy (RIT). RIT uses target-specific monoclonal antibodies combined with a radionuclide to deliver radiation into the tumor [5–7]. Up to now, available RIT treatments are based on conjugates made of one radioactive atom per vector. In order to improve its efficacy, the antibody could be linked to a nanoparticle, containing a larger number of radioactive atoms rather than a single one [8]. Its much higher specific activity is counterbalanced by a more complex radiochemistry. The coating of the

M. Crespin · C. Michiels (✉)
Unité de Recherche en Biologie Cellulaire, NARILIS, University of Namur-FUNDP, URBC, 61 rue de Bruxelles, 5000 Namur, Belgium
e-mail: carine.michiels@fundp.ac.be

N. Moreau · S. Lucas
Research Center in Physics of Matter and Radiation (PMR), NARILIS, University of Namur-FUNDP, Namur, Belgium

B. Masereel
Drug Design and Discovery Center, NARILIS, University of Namur-FUNDP, Namur, Belgium

O. Feron
Unit of Pharmacology and Therapeutics, Université catholique de Louvain, UCL-FATH, Brussels, Belgium

B. Gallez
Biomedical Magnetic Resonance Unit, Université catholique de Louvain, UCL-CMFA, Brussels, Belgium

T. Vander Borght
Division of Nuclear Medicine, Mont-Godinne University Hospital, Université catholique de Louvain, Yvoir, Belgium

nanoparticle with a surface-functionalized material may be used to build this conjugate. The latter should however not induce an inflammatory response once injected to avoid compromising the potential therapeutic effect.

This work is aimed to assess such a risk by testing, on endothelial cells, the biocompatibility of different materials that could be used as the interface between the nanoparticle and the monoclonal antibody. Among the different coating processes available, the magnetron sputtering deposition process [9–11] was selected because the radioactive nanoparticles will also be produced by vacuum based technique [12]. The inclusion of all steps in the same reactor spares time [13], which may become critical when using short half-life radioactive materials. Cell adhesion is dependent on the surface properties of materials [14] such as high wettability [15] and basic property [16] which are able to increase their biocompatibility. Furthermore, coating may require chemical functionalization for antibody immobilization [17] usually using amine functions. Two different nitrogen-functionalized coatings can be obtained either by plasma treatment carried out under nitrogen or by plasma polymerization of allylamine [18]. The goal of this study is to assess the biocompatibility of the plasma-synthesized materials themselves, deposited on flat substrates. It is well known that the PVD deposition mechanisms at the early stages of the film growth are highly dependant on the substrate [19]. In some cases, nanometer-ranged films can grow as islands instead of continuous thin layers. Therefore, the deposited layer does not entirely cover the substrate, and its intrinsic roughness is strongly modified by the plasma deposition. A way to avoid those issues is to make a rather thick deposit (>50 nm) onto the glass coverslips. This is the option chosen in this work.

In this work, we studied the biocompatibility of these plasma-deposited materials with and without amine-functionalization using endothelial cells. Endothelial cells were chosen because they will be targeted by RIT using antibodies coupled to nanoparticles.

2 Materials and methods

2.1 Coating synthesis

All materials were deposited on glass coverslips thanks to a Physical Vapor Deposition System (PVD). It consists of a vacuum chamber equipped with 2″ unbalanced-magnetron sputtering guns, powered by supply configured in DC or pulsed bipolar mode. The plasma excitation mode was chosen in order to obtain the best deposition rate and plasma stability as well as the least porous material. The different deposition conditions are listed in Table 1. Two cathodes were used: carbon for the carbon or silicon for the silicon based coatings respectively (99.9% purity for each). Coating thickness was about 100 nm for all samples. Carbon, CH_x and SiO_x are the nitrogen-free materials studied in this work. They were synthesized in either DC (direct current) for C and PPAA coatings, or pulsed bipolar ($T_{on+} = T_{on-}$: 10 µs, $T_{off+} = T_{off-}$: 50 µs for CH_x, T_{on+}: 20 µs, T_{on-}: 90 µs, T_{off+}: 5 µs, T_{off-}: 5 µs for SiO_x). PPAA coatings were produced as described in [20]. The properties of carbon and CH_x films have been previously characterized [21]. This coating is amorphous. The hydrogen content of the CH_x film is about 55%, and its density is closed to 1.2 g/cm^3. They are described as a highly branched and highly cross-linked hydrocarbon network with a fairly large number of free radicals. When air-exposed, they become slightly oxidized as revealed by the presence of C=O stretching band measured by FTIR. The oxygen bulk concentration of SiO_x films has been measured by Rutherford Backscattering Spectrometry (RBS) and is the one of SiO_x compound. In order to functionalize these coatings with nitrogen, N_2 gas was injected into the chamber during the plasma deposition process, either pure (CN_x) or mixed with argon (CH_xN_y) following the parameters listed in Table 1.

Plasma Polymerized AllylAmine (PPAA) coatings were obtained by generating a discharge in pure allylamine

Table 1 Process parameters for deposited coatings

Name of the deposited material	Composition of the target	Power (W)	Power supply mode	Deposition pressure (mbars)	Atmosphere composition
C	C	350	DC	3×10^{-3}	Ar (100%)
CN_x	C	350	DC	2×10^{-3}	N_2 (100%)
CH_x	C	100	Pulsed (kHz)	2×10^{-3}	C_2H_2 (100%)
CH_xN_y	C	100	Pulsed (kHz)	4×10^{-3}	C_2H_2 (35%); N_2 (65%)
PPAA	C	20	DC	3×10^{-2}	C_3H_7N (100%)
SiO_x	Si	350	Bipolar pulsed (kHz)	3×10^{-3}	Ar (70%); O_2 (30%)
SiO_xN_y	Si	350	Bipolar pulsed (kHz)	4×10^{-3}	Ar (70%); N_2 (30%)

vapor, according to the procedure described by Lucas et al. [20]. Their properties depend on the power fed into the plasma: here, we generated coatings that are $C_{0.45}H_{0.32}N_{0.13}O_{0.1}$. To achieve sterile conditions, the coverslips were autoclaved prior to their utilization for cell seeding (during 20 min at 121°C and 16 Psi). The stability of allylamine deposit is high after autoclaving with only minor changes in nitrogen composition and wettability [16].

2.2 Plasma-coated substrate characterization

After the deposition and the sterilization processes, all coated substrates were characterized by XPS in order to probe for the chemical composition of their extreme surface. Measurements were performed with a SSX-100 spectrometer (Surface Science Instruments), with incident X-Ray beam of 1486.6 eV (Al K_α), and without any ionic etching prior the analysis. To determine the stoichiometry, all areas of peaks were normalized with appropriate Scoffield factors given by the spectrometer manufacturer. Evidence of the chemical functions (especially the presence of amine groups) of the PPAA layer was obtained by chemical derivatization of amine groups into imine with pentafluorobenzaldehyde (PFBA) [22]. The reaction was carried out in ethanol for 15 h (50°C, nitrogen-flushed reactor). Then, the substrate with the PPAA layer was thoroughly washed by different organic solvents (ethanol, dichloromethane, acetone and hexane) under ultrasonication, in order to release the PFBA molecules non-covalently bound to the surface. Finally, the amine group concentration was obtained by measuring the fluorine atomic concentration on derivatized samples by XPS, normalized by the carbon peak area. The surface amine concentration (in atomic percents) was determined by the formula: $[NH_2] = \frac{[F]/5}{[C]-7[F]/5} \times 100$, adapted from Choukourov et al. [23]. The layer of PPAA was also characterized by Nuclear Reactions Analysis (NRA), using a 2.385 MeV ^{3}He beam [20]. This technique provides the measurement of atomic concentrations of all elements present in the entire layer, whereas the XPS measurements only give information coming from the extreme surface of the layer. Wettability of the substrates was characterized by contact angle measurements, carried out with VCA 2500 XE system. The measurements were performed, after being washed in ethanol, at room temperature with droplets of ca. 0.5 µl of ultrapure water.

2.3 Cell culture

The human endothelial cell line EAhy926 was kindly provided by Prof. C. Edgell (Pathology Department, University of North Carolina) [24]. Cells were maintained in culture at 37°C under 5% CO_2 and 95% air atmosphere, in 75 cm^2 polystyrene flasks (Costar) with Dulbecco's Modified Eagle Medium (DMEM, Gibco) (4.5 g/l D-glucose) containing $NaHCO_3$ (1.5 g/l) but no pyruvate and 10% foetal calf serum. For the experiments, cells were harvested by trypsinization and seeded in 24-well plates onto the different coverslips at a density of 10,000 cells per well. They were then incubated for different times in complete medium.

2.4 Coomassie blue staining

The morphology of cells seeded on the different substrates was assessed after cell protein staining with Coomassie Blue. Briefly, EAhy926 endothelial cells were first washed twice with PBS, and fixed with 3.7% PFA in distilled water for 10 min at RT. Then, they were permeabilized with 70% ethanol in distilled water for 10 min at RT and dried at 37°C. The cells were finally stained with Coomassie Blue for 30 s, washed with distilled water and dried at 37°C, before being photographed with an inverted microscope (Labovert FS, Leitz).

2.5 Cell viability assay

To assess cell proliferation/viability on the different substrates, an MTT assay was performed using EAhy926 endothelial cells. Six days after plating, 500 µl of MTT solution (2.5 mg/ml of [3-(4,5-diMethylThiazol-2-yl)-2,5-diphenyTetrazolium bromide], Sigma in PBS) were added to the culture medium for 2 h at 37°C. The medium was then removed and 1 ml of lysis solution (2 volumes of SDS 30% and 1 volume of *N,N*-dimethyl-formamide) was added to the cells for 1 h at 37°C on a rotating plate (80 rpm) before the optical absorbance measurement using a plate reader (BIO-RAD) at a wavelength of 570 nm.

2.6 Immunofluorescence staining

The EAhy926 endothelial cells were fixed with 4% paraformaldehyde in PBS for 10 min at 20°C, and washed three times with PBS. They were then permeabilized with 1% Triton-X-100 (Sigma) in PBS for 5 min. They were then washed three times with PBS-BSA (Sigma). For actin staining, cells were incubated with Alexa Fluor 546 phalloïdin (Molecular Probes) at 1:50 dilution, overnight at 4°C. For focal adhesion plaques staining, cells were incubated with the primary antibody diluted in PBS-BSA, overnight at 4°C. The next day, cells were washed three times with PBS-BSA and incubated for 1 h in the presence

of the secondary antibody in PBS-BSA at 20°C. For both stainings, after three washes in PBS, nuclei were stained with To-Pro-3 (Molecular Probes) diluted (1:80) in PBS-RNase (2 mg/ml). The samples were again washed three times before being embedded in Mowiol (Aldrich) and photographed with a confocal microscope TCS (Leica SP1) using a 40× objective and a constant photomultiplier. Mouse anti-Vinculin monoclonal antibody (Sigma) was used at 1:800 dilution. Alexa Fluor 488 goat anti-mouse IgG conjugate (Molecular Probes) was used at 1:1000 dilution.

2.7 Scanning electron microscopy

The samples were fixed with 2% glutaraldehyde in 0.1 M cacodylate buffer pH 7.4 overnight at 4°C. Samples were then washed three times for 15 min in 0.1 M cacodylate buffer pH 7.4 containing 7.5% sucrose. The specimens were then dehydrated in a series of increasing concentrations of acetone, critical-point dried by use of liquid CO_2, and sputter coated with gold. Samples were examined with a scanning electron microscope (SEM) Philips XL-20 operating at an accelerating voltage of 15 kV and photographs were taken.

2.8 Signal chip human cytokine array

SignalChip Human Cytokine microarrays (Eppendorf Array Technologies) were used to analyze the protein level of 20 human cytokines, namely eotaxin, GM-CSF, IFN, IL-1α, IL-1β, IL-2, IL-4, IL-6, IL-8, IL-10, IL-12p40, IL-12p70, IL-17, IP-10, MIP-1α, MIP-1β, RANTES, TNFα, TNF-RI and TNF-RII. The assay is based on a sandwich ELISA, where capture antibodies are spotted on glass slides in an array format. Samples are contacted with the array, and detection is performed using labeled detection antibodies. Positive and negative controls are included to normalize the data, and calibration curves constructed from known amounts of purified cytokines are used to generate quantitative data. Arrays were contacted with 8.7 µl of sample diluted 10 times and detection was performed in fluorescence, according to the manufacturer's protocol. Scanning was performed using a ScanArray scanner, and signals were quantified using the Imagene software (Perkin Elmer). Data analysis was performed using the data analysis software provided with the arrays.

2.9 Statistical analysis

One way analysis of variance (ANOVA) with post hoc pairwise comparison using Holm-Sidak method was performed using SigmaStat.3 software.

3 Results

3.1 Coating characteristics

All glass samples coated by magnetron sputtering deposition were analyzed by XPS. The elemental composition (in atomic percentage) of the coating surface was not affected by autoclaving (Table 2). The use of the reactive nitrogen atmosphere influenced the atomic composition of the deposited layers, compared to the conventional sputtering conditions: the [N]/[C] ratio varies from 0.01 to 0.07 for CH_x and the [N]/[Si] ratio from 0.01 to 0.02 for SiO_x (Table 3). The strongest modification induced by the N_2 functionalization was observed for the amorphous C synthesis. In this case, the [N]/[C] ratio increased from 0.017 to 0.26 if the non-reactive sputtering gas (Ar) was replaced by pure nitrogen during the sputtering process. This [N]/[C] ratio is slightly higher than the results reported by Neidhardt et al. [25], where a similar experiment produced CN_x films, with [N] values between 16 and 25 at.% while the [N] content was 18.8% in our experiments.

The PPAA-coated sample also showed a high atomic [N]/[C] ratio (15%). The derivatization technique applied on this sample gave evidence for the presence of reactive –NH_2 functions on the surface even after the autoclaving. Using the formula described here above, the surface

Table 2 Atomic composition of autoclaved materials, prior seeding the cells

Name of the deposited material	[C] (at.%)	[N] (at.%)	[O] (at.%)	[Si] (at.%)
C	93.7	1.6	4.7	–
CN_x	71.6	18.8	9.6	–
CH_x	93	1	6	–
CH_xN_y	85.9	5.8	8.3	–
PPAA	78.3	11.4	10.3	–
SiO_x	17	0.7	52.4	29.9
SiO_xN_y	21.5	1.5	49.8	27.2

Table 3 Effect of nitrogen functionalization on the composition of the PVD coatings probed by XPS

Name of the deposited material	[N]/[C]	[N]/[Si] + [O]
C	0.02	–
CN_x	0.26	–
CH_x	0.01	–
CH_xN_y	0.07	–
PPAA	0.15	–
SiO_x	–	0.01
SiO_xN_y	–	0.02

Results are given in atomic concentrations

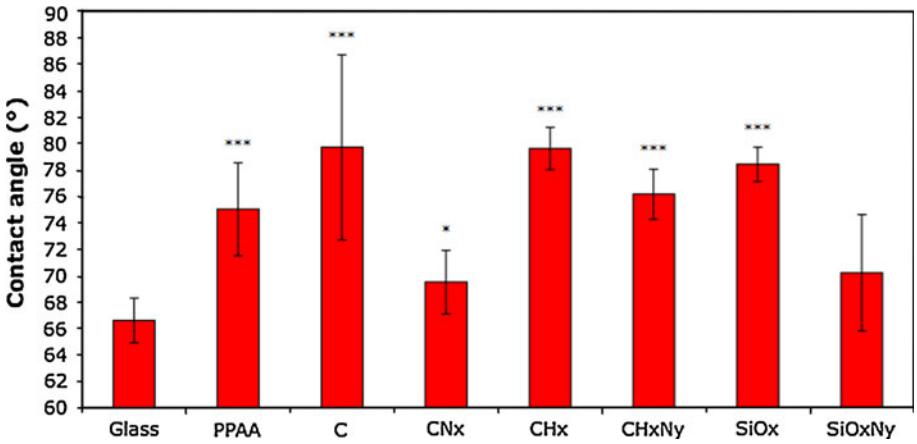

Fig. 1 Contact angle measurements for plasma-deposited substrates. A droplet of 500 µl of ultrapure water was added on the coverslip before measurement. Results are expressed as means ± 1 SD ($n = 3$). *; ***: $P < 0.05$; $P < 0.001$ versus glass

concentration of amine was determined as 1.3% under the deposition conditions given in Table 1. The stoechiometry of this material (bulk measurements) probed by NRA technique is $CH_{0.7}N_{0.29}O_{0.2}$ [20]. The value of [N]/[C] ratio obtained by NRA (28%) averaged for the entire layer was slightly higher than the one measured by XPS.

On the whole set of plasma-deposited materials, contact angle measurements showed that the nitrogen functionalization always decreased the contact angle of water drops (Fig. 1). The contact angle value was 67° for glass (flat alkali silica glass) which is similar to values obtained by Huber et al. [26]. The largest modification of the mean contact angle induced by the nitrogen functionalization was observed for the amorphous C material (decrease from 80 to 69°). It was slightly lower for SiO_x material (decreasing from 78 to 70°). These results are consistent with results reported by Mardare et al. [27], showing that nitrogen incorporation in the layer can potentially lead to a more hydrophilic surface, compared to unfunctionalized material.

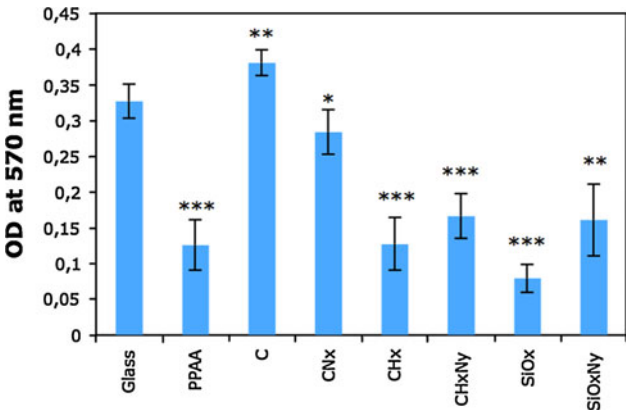

Fig. 2 Effect of deposit chemical composition on cell number. The EAhy926 endothelial cells were seeded on the different materials: Glass, PPAA, CH_x, CH_xN_y, C, CN_x, SiO_x and SiO_xN_y. Six days later, cell metabolic activity assessing overall cell number was measured using a MTT assay as described in "Materials and methods". Results are expressed as means ± 1 SD ($n = 3$). *; **; ***: $P < 0.05$; $P < 0.01$; $P < 0.001$ versus glass

3.2 Cell viability

The first way to measure the innocuousness of the different materials coating the glass coverslips was to measure EAhy926 endothelial cell viability/proliferation. This was achieved by performing a MTT assay 6 days after the cells were seeded on the different deposited materials.

The number of viable EAhy926 cells was the highest on C-coated coverslips (Fig. 2). It was also high on CN_x and on glass coverslips. However, cell number was much lower for EAhy926 cells grown on PPAA, CH_x, CH_xN_y, SiO_x and SiO_xN_y (Fig. 2).

3.3 Cell morphology

In order to confirm these results, we observed cell morphology, attachment and spreading on the different coverslips. Cell morphology was first observed by staining cell proteins with Coomassie blue (Fig. 3). EAhy926 endothelial cells were incubated 4 or 24 h on the differently coated coverslips. After 4 h, cells adhered the best to C and CN_x. On glass, PPAA, CH_x and CH_xN_y, only few cells were well attached to the coverslips, the majority being round-shaped. On SiO_x and SiO_xN_y, most of the cells were round. After 24 h, cells had time to adhere to all coverslips (as shown for C) except to the ones coated with SiO_x or SiO_xN_y (Fig. 3).

We also visualized cell morphology using scanning electron microscopy (Fig. 4). Cells started to adhere to the different coverslips after 4 h. On SiO_x and SiO_xN_y, some cells started to adhere to the coverslips but others engaged apoptosis. However, after 24 h most cells were well attached on all the materials tested.

3.4 Cell attachment and spreading

The cytoskeleton provides the cell cytoplasm with structure and shape. It enables cellular motility by the formation of

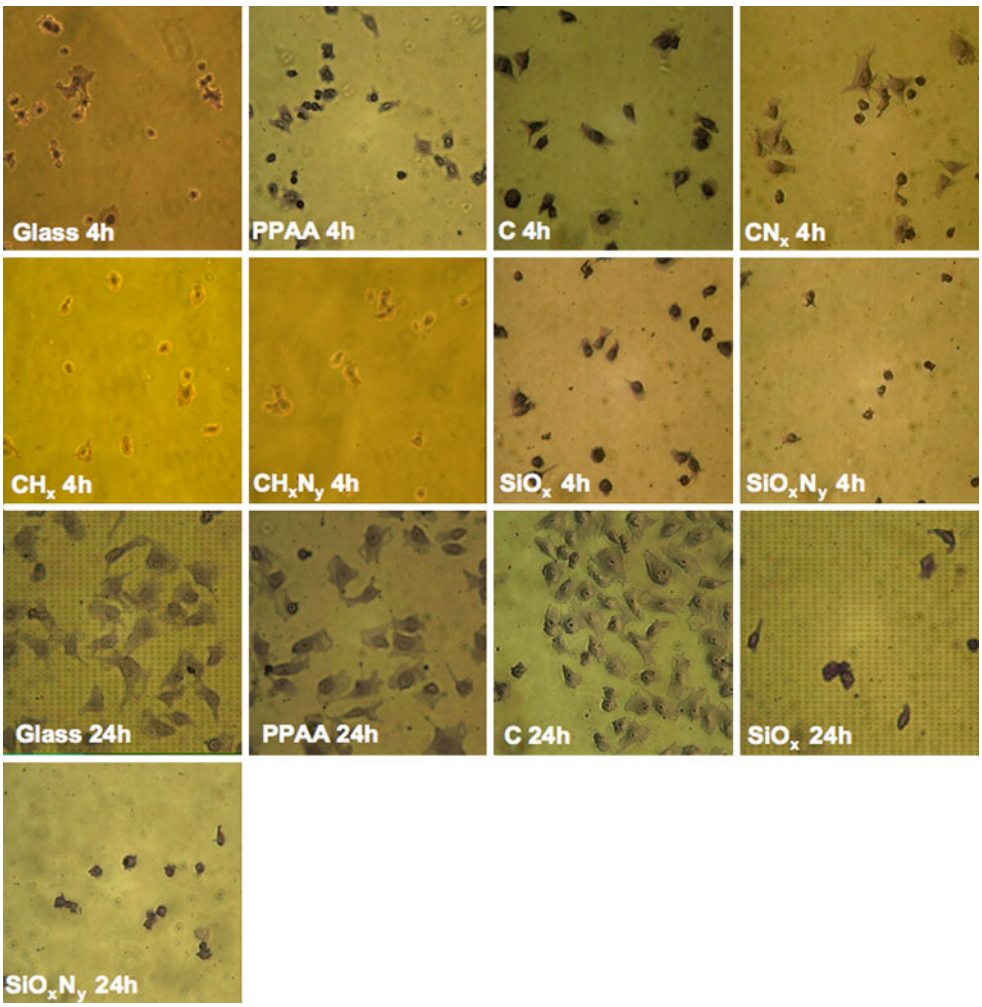

Fig. 3 Effect of deposit chemical composition on overall endothelial cell morphology visualized by Coomassie Blue staining. The EAhy926 endothelial cells were seeded on the different materials: Glass, PPAA, CN_x and SiO_xN_y. Four hours or 24 h later, they were stained with Coomassie Blue to assess their overall morphology and observed in phase contrast microscopy

cytoplasmic protuberances like lamellipodia, and participates in cell-to-cell or cell-to-matrix adhesion.

Cytoskeleton formation was observed in EAhy926 endothelial cells by staining actin protein (Fig. 5). After 4 h incubation on C, cells were well spread and had already developed a well-structured cytoskeleton. On the contrary, 4 h after seeding on SiO_x or SiO_xN_y, most cells were still round and did not form any actin fibers yet. On the other surfaces (i.e., glass, PPAA, CH_x and CH_xN_y), the cytoskeleton was under formation.

Twenty-four hours after seeding, cells adhered to all surfaces. They spread more on C and CN_x, and lesser on SiO_x and SiO_xN_y.

Focal adhesion plaques are parts of the cellular membrane that serve for the anchorage of the cell to the extracellular matrix and that participate to cellular motility. Vinculin is a cytoskeletal protein associated with focal adhesion plaques, involved in anchoring the actin cytoskeleton to the cellular membrane.

We observed focal adhesion plaques in EAhy926 endothelial cells by staining vinculin protein (Fig. 6). Four hours after seeding cells on glass, C and CN_x, cells were well spread and had already formed some focal adhesion plaques. On the other surfaces, most cells were still round and only a few focal adhesion plaques were visible. After 24 h incubation, cells adhered to all surfaces. They spread more on C and CN_x (a lot of focal adhesion plaques were observed), and lesser on SiO_x and SiO_xN_y, as previously observed for actin staining.

3.5 Cell activation

Some materials allow cell spreading and proliferation but induce an inflammatory reaction which could lead to adverse

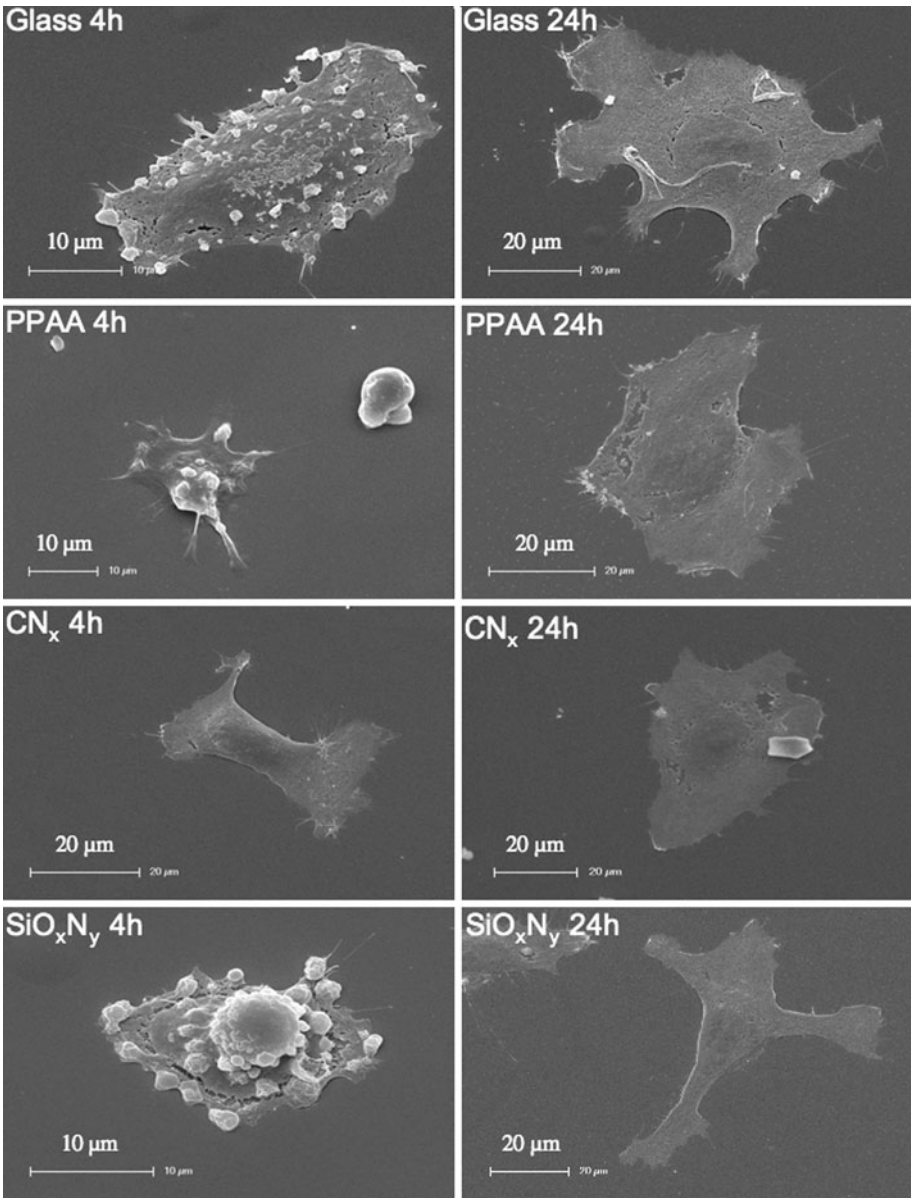

Fig. 4 Effect of deposit chemical composition on overall endothelial cell morphology visualized by scanning electronic microscopy. The EAhy926 endothelial cells were seeded on the different materials: Glass, PPAA, CN_x and SiO_xN_y. Four hours or 24 h later, cells were fixed, dehydrated, critical-point dried and sputter coated with gold. Overall cell morphology was then visualized by scanning electronic microscopy

effects. In order to evaluate endothelial cell activation, we assayed the amount of pro-inflammatory cytokines secreted in the extracellular medium, using a low-density protein microarray. Interleukin-8 (IL-8) was the cytokine secreted in the highest amounts in all conditions. After 3 days incubation on glass, C or CN_x, the amount of IL-8, IL-6 and interferon-γ released by EAhy926 endothelial cells was approximately twice lower than if seeded onto the other materials (Fig. 7). On the other hand, PPAA coating induced an increase in seven of the eight cytokines detected in the medium, indicating that it provoked endothelial cell activation.

3.6 Relation of cell proliferation to surface properties

The observed MTT proliferation assay data were put in the perspective of the measured surface characteristics (Fig. 8). A clear correlation between the water-contact angle and cell proliferation can be observed, except for the carbon coating. On the other hand, no correlation could be noted when wettability was put in relation with IL-8 secretion (data not shown).

4 Discussion

In this work, we produced a series of un-functionalized and nitrogen-functionalized materials that can be utilized to coat nanoparticles to be used in RIT.

In our team, we have developed a full vacuum process, able to automatically synthesize coated nanoparticles and, at the end of the process, to recover them in water [13]. The nanoparticles themselves are produced by DC magnetron

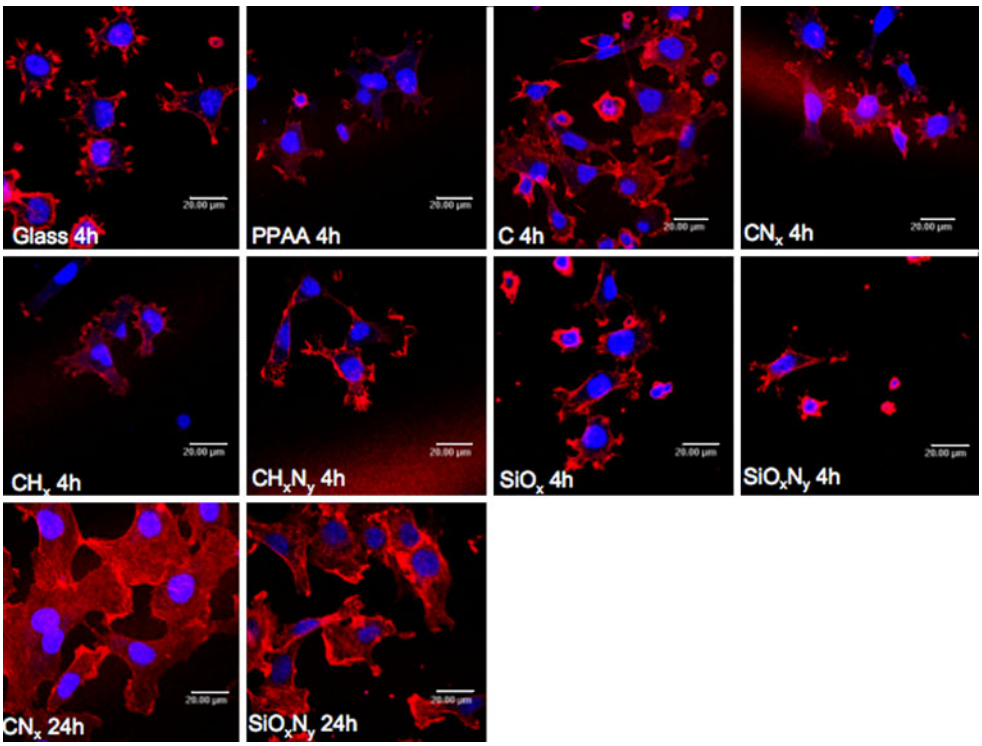

Fig. 5 Effect of deposit chemical composition on actin stress fibers formation in endothelial cells. The EAhy926 endothelial cells were seeded on the different materials: Glass, PPAA, CH_x, CH_xN_y, C, CN_x, SiO_x and SiO_xN_y. Four hours or 24 h later, cells were fixed, permeabilized and stained for actin using Alexa Fluor 546 phalloidin (*red*). Nuclei were detected with To-Pro-3 (*blue*). Observation was performed using a confocal microscope with a constant photomultiplier (Color figure online)

sputtering, onto a NaCl substrate. After the synthesis, these nanoparticles are coated in the same vacuum reactor, by Plasma-Enhanced Chemical Vapour Deposition, carried out in similar conditions than described here. In the final step, the substrate is dissolved by dipping it in pure water: the coated nanoparticles lying on the surface of the substrate are therefore released in water. With this method, we succeeded to collect, in water, nanoparticles as isolated nanoparticles with a diameter ranging from 10 to 20 nm. We showed that the plasma coating plays two roles (1) It prevents post-synthesis aggregation of the nanoparticles when they are transferred in water (2) Thanks to the presence of reactive moieties present at the extreme surface of the coating, it makes possible the covalent grafting of some biomolecules (such as antibodies) by conventional surface chemistry processes.

This series of un-functionalized and nitrogen-functionalized materials that can be utilized to coat nanoparticles was analyzed for its interaction with endothelial cells with respect to a number of cell adhesion and growth parameters.

4.1 Coating biocompatibility

All together, the results show that, among the surface coatings tested, glass, C and CN_x were the most biocompatible substrates; PPAA, CH_x and CH_xN_y were intermediate and SiO_x and SiO_xN_y were the most toxic materials, both for cell proliferation and cell attachment. Indeed, on a material that promotes cell proliferation, cells spread out in order to have the most contact with the material. Therefore, cells develop their cytoskeleton by forming actin microfilaments and focal adhesion plaques to better attach to the material. On the other side, on a material that does not promote cell proliferation, cells adopt a round shape and are unable to spread. This kind of weak cell-material interaction can eventually lead to cell death. A strong correlation between cell spreading and cell proliferation was observed in this work.

4.2 Influence of hydrophilicity

It is recognized that the attachment and spreading of cells on materials largely depends on surface characteristics such as hydrophilicity/hydrophobicity, surface charge, roughness and rigidity [28]. Results from Fig. 8 show a good correlation between contact angle and cell number i.e., the more hydrophilic the coating, the more cells were obtained after 6 days incubation. These results are in good accordance with published data. Indeed, plasma-treated polystyrene surfaces with contact angle values from 40° to 75° well sustain endothelial cell proliferation while they

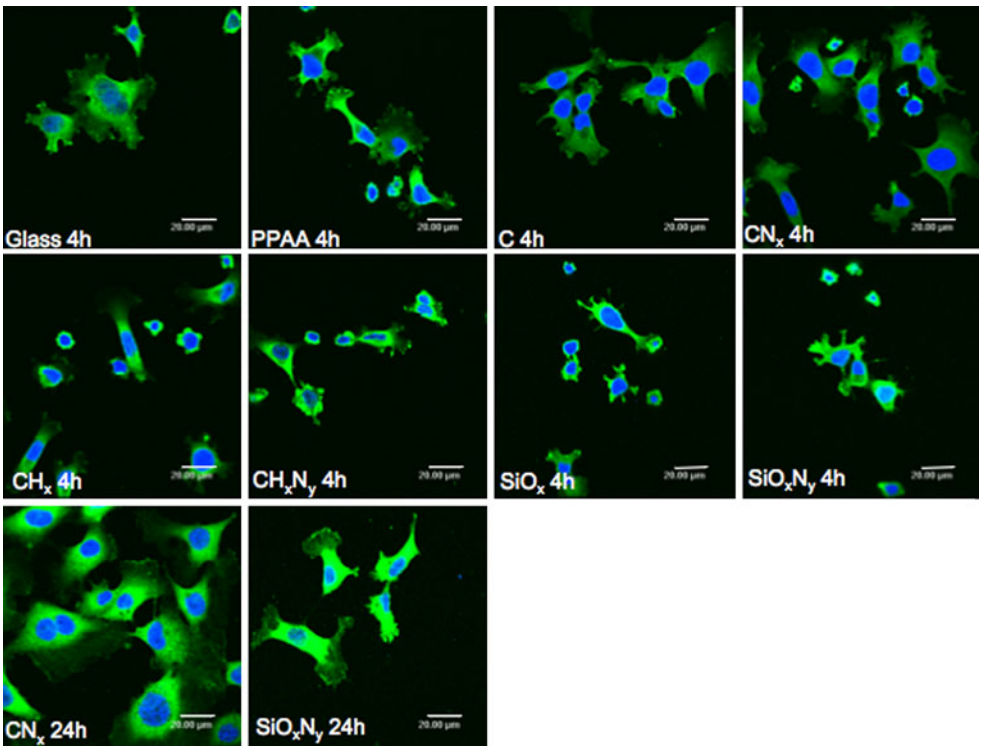

Fig. 6 Effect of deposit chemical composition on focal adhesion plaque formation in endothelial cells, visualized by staining vinculin. The EAhy926 endothelial cells were seeded on the different materials: Glass, PPAA, CH_x, CH_xN_y, C, CN_x, SiO_x and SiO_xN_y. Four hours or 24 h later, cells were fixed, permeabilized and stained for vinculin using a specific antibody (*green*). Nuclei were detected with To-Pro-3 (*blue*). Observation was performed using a confocal microscope with a constant photomultiplier (Color figure online)

become toxic for contact angle values of 80° [29]. We indeed also observed that endothelial cell number was the lowest when seeded on coating with contact angle values higher than 75°. Similarly, the optimal contact angle value that sustain neurite growth from the rat pheochromocytoma cells (PC-12) attached on polyethylene surfaces with different wettability is aroung 58° and decreases sharply for values higher than 70° [30]. The only exception in our data is the result obtained for carbon coating which displayed a very high contact angle value but which seemed to be very biocompatible. As mentioned in the "Materials and methods", the incorporation of oxygen atoms in this coating during its synthesis may explain this observation.

It has to be noted that other factors than hydrophilicity may influence the wettability. Indeed, direct comparisons of contact angle values between different materials are irrelevant if the surface roughness is different. The wettability is known to be influenced by both surface roughness [31]—not investigated in this work—and surface chemistry. The use of various plasma deposition parameters (such as power, pressure,…) for the different materials potentially leads to different surface topologies. Since the cell adhesion is negligibly affected by the surface roughness [32], differences of surface topology can explain inconsistencies observed between hydrophilicity and biocompatibility. This still needs further characterization here.

4.3 Influence of charges

Moreover, other parameters than hydrophilicity also influence cell adhesion including the presence of polar and/or charged groups on the surface [33–35]. Cells grow more easily on positively charged surface while cell attachment and proliferation are inhibited by negative charges [36]. The positive charges may improve cell adhesion because plasma membrane carries a net negative charge [34]. However, no such correlation was observed in our work since CN_x allowed less cell spreading and less cell proliferation that the corresponding unfunctionalized C. This may be explained by the relatively low content of amine groups when compared to the poly-lysine coating usually used to increase cell adhesion. Moreover, the protonated amine groups at physiological pH of the PPAA coating would seem to be more favorable for cell growth. However, the results show that PPAA coating neither sustained high cell spreading nor proliferation, in the experimental conditions used here. These results are in contrast to the ones obtained by Hamerli et al. [37] that showed strong adhesive properties of PPAA for skin fibroblasts. This

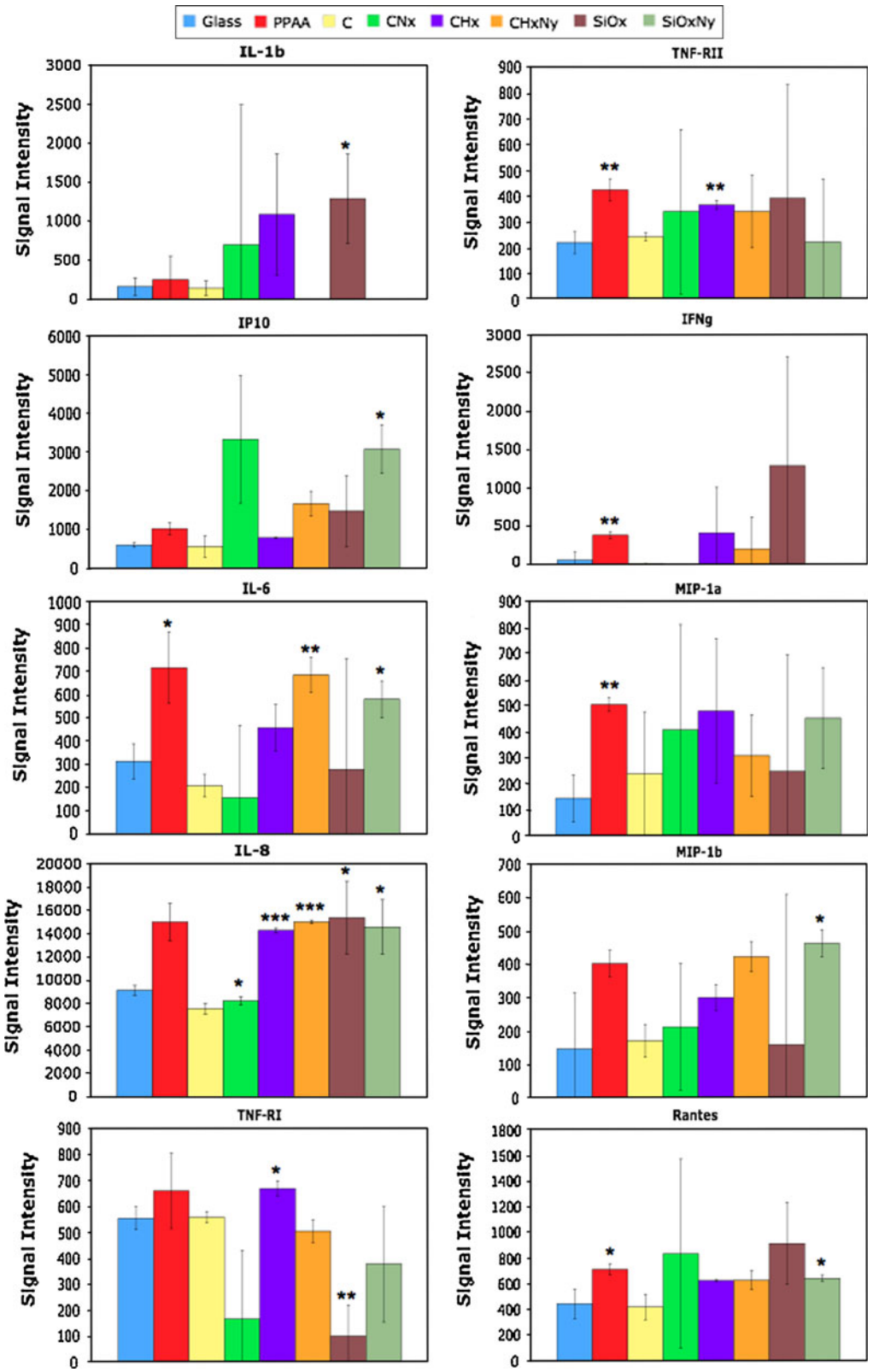

Fig. 7 Effect of deposit chemical composition on pro-inflammatory cytokines secretion. The EAhy926 endothelial cells were seeded on the different materials: Glass, PPAA, CH_x, CH_xN_y, C, CN_x, SiO_x and SiO_xN_y. Three days later, the SignalChip Human Cytokine array was used to detect and quantify the amount of cytokines secreted by the cells in the medium, as described in "Materials and methods". Graphs are presented only for the cytokines that have been detected in the medium. *; **; ***: $P < 0.05$; $P < 0.01$; $P < 0.001$ versus glass

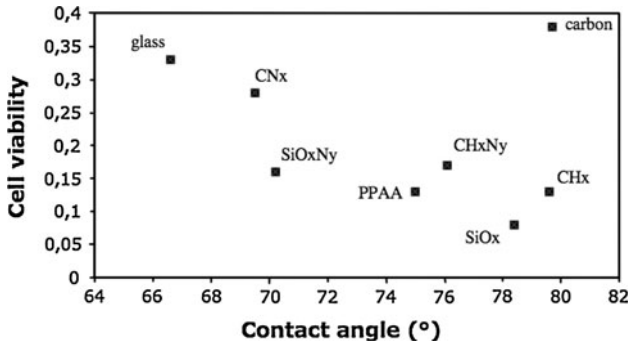

Fig. 8 Relation between material surface wettability and cell proliferation. Wettability data are given in contact angle (°) from Fig. 1 and cell proliferation are MTT data from Fig. 2

discrepancy may be due to difference in the cell type, as it has been already described for wettability. Indeed, differences in cell growth pattern against wettability are clearly recognized for each cell type [38].

4.4 Influence of protein adsorption

This situation is further complicated by protein adsorption to the surface prior to cell attachment. Cells are seeding in medium supplemented with serum that contains numerous proteins able to adsorb on the glass or the coating surface. In addition, cells per se synthesize and secrete abundant extracellular matrix proteins, collagen being the most predominant one [16, 39]. All these proteins are able to sustain cell adhesion and spreading to some extent. According to the various physical and chemical parameters of the coatings, protein adsorption may adopt different topologies forming no, small or large aggregates that strongly influences cell adhesion [40]. Further studies are warranted to understand whether difference in the topology of adsorbed proteins may explain those we observed in biocompatibility according to the nature of the coatings.

5 Conclusion

The results show that, among the materials tested, C and CN_x were the most biocompatible substrates while SiO_x and SiO_xN_y were the most toxic materials. A correlation could be observed between wettability and cell proliferation except for C coated surface, indicating that more complex processes than hydrophilicity alone are taking place that affect cell functions.

Acknowledgments This research (Targan Project, grant No. 516071) is supported by the Walloon Region (Belgium). We thank Dr. Edgell for having provided the EAhy926 endothelial cells. O. Feron is Research Director of FNRS (National Funds for Scientific Research, Belgium).

References

1. Raez LE, Fein S, Podack ER. Lung cancer immunotherapy. Clin Med Res. 2005;3:221–8.
2. Sridhar SS, Shepherd FA. Targeting angiogenesis: a review of angiogenesis inhibitors in the treatment of lung cancer. Lung Cancer. 2003;42(Suppl 1):S81–91.
3. Weynants P, Marchandise FX, Sibille Y. Pulmonary perspective: immunology in diagnosis and treatment of lung cancer. Eur Respir J. 1997;10:1703–19.
4. Tsuboi M, Ohira T, Saji H, Miyajima K, Kajiwara N, Uchida O, Usuda J, Kato H. The present status of postoperative adjuvant chemotherapy for completely resected non-small cell lung cancer. Ann Thorac Cardiovasc Surg. 2007;13:73–7.
5. Rao AV, Akabani G, Rizzieri DA. Radioimmunotherapy for Non-Hodgkin's Lymphoma. Clin Med Res. 2005;3:157–65.
6. Verel I, Visser GW, van Dongen GA. The promise of immuno-PET in radioimmunotherapy. J Nucl Med. 2005;46(Suppl 1):164S–71S.
7. Macklis RM, Pohlman B. Radioimmunotherapy for non-Hodgkin's lymphoma: a review for radiation oncologists. Int J Radiat Oncol Biol Phys. 2006;66:833–41.
8. Bouchat V, Nuttens VE, Lucas S, Michiels C, Masereel B, Feron O, Gallez B, Vander Borght T. Radioimmunotherapy with radioactive nanoparticles: first results of dosimetry for vascularized and necrosed solid tumors. Med Phys. 2007;34:4504–13.
9. He Y, Bi L, Feng JY, Wu QL. Properties of Si-rich SIO_2 films by RF magnetron sputtering. J Cryst Growth. 2005;280:352–6.
10. Angleraud B, Tessier PY. Improved film deposition of carbon and carbon nitride materials on patterned substrates by ionized magnetron sputtering. Surf Coat Technol. 2004;180–181:59–65.
11. Diesselberg M, Stock HR, Zoch HW. Tribological performance of reactively sputtered a-C:H coatings in ambient air and aqueous environment. Plasma Process Polymers. 2007;4(S1):205–9.
12. Lucas S, Hofferlin E. Radioactive Rh wire as a source for new nanomaterials. Nucl Instr Meth Phys Res B. 2007;580:262–5.
13. Moreau N, Michiels C, Masereel B, Feron O, Gallez B, Vander Borght T, Lucas S. PVD synthesis and transfer into water-based solutions of functionalized gold nanoparticles. Plasma Process Polymers. 2009;6:S888–92.
14. Anselme K. Osteoblast adhesion on biomaterials. Biomaterials. 2000;21:667–81.
15. Webb K, Hlady V, Tresco PA. Relative importance of surface wettability and charged functional groups on NIH 3T3 fibroblast attachment, spreading, and cytoskeletal organization. J Biomed Mater Res. 1998;41:422–30.
16. Harsch A, Calderon J, Timmons RB, Gross GW. Pulsed plasma deposition of allylamine on polysiloxane: a stable surface for neuronal cell adhesion. J Neurosci Methods. 2000;98:135–44.
17. Kurosawa S, Kamo N, Aizawa H, Muratsugu M. Adsorption of 125I-labeled immunoglobulin G, its F(ab′)2 and Fc fragments onto plasma-polymerized films. Biosens Bioelectron. 2007;22:2598–603.
18. Lejeune M, Bretagnol F, Ceccone G, Colpo P, Rossi F. Microstructural evolution of allylamine polymerized plasma films. Surf Coat Technol. 2006;200:5902–7.
19. Luth H. Solid surfaces, interfaces and thin films. Springer Book; 2001.
20. Lucas S, Genard G, Michiels C, Masereel B, Feron O, Gallez B, Vander Borght T, Moreau N. Production and preliminary characterization of CD plasma polymerized allylamine film (PPAA) by NRA, ERD and XPS. Nucl Instr Meth Phys Res B. 2008;266:2494–7.
21. Vanden Brande P, Lucas S, Winand R, Weymeersch A, Renard L. Determination of the chemical and physical properties of

hydrogenated carbon deposits produced by DC magnetron reactive sputtering. Surf Coat Technol. 1994;68–69:656–61.
22. Moon JH, Shin JW, Kim SY, Park JW. Formation of uniform aminosilane thin layers: an imine formation to measure relative surface density of the amine group. Langmuir. 1996;12:4621–4.
23. Choukourov A, Biederman H, Slavinska D, Trchova M, Hollander A. The influence of pulse parameters on film composition during plasma polymerization of diaminocyclohexane. Surf Coat Technol. 2003;174:863–6.
24. Edgell CJ, McDonald CC, Graham JB. Permanent cell line expressing human factor VIII-related antigen established by hybridization. Proc Natl Acad Sci USA. 1983;80:3734–7.
25. Neidhardt J, Hultman L, Broitman E, Scharf TW, Singer IL. Structural, mechanical and tribological behavior of fullerene-like and amorphous carbon nitride coatings. Diam Relat Mater. 2004;13:1882–8.
26. Huber G, Mantz H, Spolenak R, Mecke K, Jacobs K, Gorb SN, Arzt E. Evidence for capillarity contributions to gecko adhesion from single spatula nanomechanical measurements. Proc Natl Acad Sci USA. 2005;102:16293–6.
27. Mardare D, Luca D, Teodorescu CM, Macovei D. On the hydrophilicity of nitrogen-doped TiO_2 thin films. Surf Sci. 2007;601:4515–20.
28. Ramires PA, Mirenghi L, Romano AR, Palumbo F, Nicolardi G. Plasma-treated PET surfaces improve the biocompatibility of human endothelial cells. J Biomed Mater Res. 2000;51:535–9.
29. van Kooten TG, Spijker HT, Busscher HJ. Plasma-treated polystyrene surfaces: model surfaces for studying cell-biomaterial interactions. Biomaterials. 2004;25:1735–47.
30. Lee SJ, Khang G, Lee YM, Lee HB. The effect of surface wettability on induction and growth of neurites from the PC-12 cell on a polymer surface. J Colloid Interface Sci. 2003;259:228–35.
31. Wenzel RN. Surface roughness and contact angle. J Phys Colloid Chem. 1949;5:1466–7.
32. Richards RG. The effect of surface roughness on fibroblast adhesion in vitro. Injury. 1996;27(Suppl 3):SC38–43.
33. Maroudas NG. Adhesion and spreading of cells on charged surfaces. J Theor Biol. 1975;49:417–24.
34. van Wachem PB, Hogt AH, Beugeling T, Feijen J, Bantjes A, Detmers JP, van Aken WG. Adhesion of cultured human endothelial cells onto methacrylate polymers with varying surface wettability and charge. Biomaterials. 1987;8:323–8.
35. Davies JE. The importance and measurement of surface charge species in cell behavior at the biomaterial interface. In: Ratner BD, editor. Surface characterization of biomaterials. Amsterdam: Elsevier; 1998. p. 219–34.
36. Lee JH, Lee JW, Khang G, Lee HB. Interaction of cells on chargeable functional group gradient surfaces. Biomaterials. 1997;18:351–8.
37. Hamerli P, Weigel T, Groth T, Paul D. Surface properties of and cell adhesion onto allylamine-plasma-coated polyethylenterephtalat membranes. Biomaterials. 2003;24:3989–99.
38. Fuse Y, Hirata I, Kurihara H, Okazaki M. Cell adhesion and proliferation patterns on mixed self-assembled monolayers carrying various ratios of hydroxyl and methyl groups. Dent Mater J. 2007;26:814–9.
39. Dewez JL, Doren A, Schneider YJ, Rouxhet PG. Competitive adsorption of proteins: key of the relationship between substratum surface properties and adhesion of epithelial cells. Biomaterials. 1999;20:547–59.
40. Satriano C, Marletta G, Carnazza S, Guglielmino S. Protein adsorption and fibroblast adhesion on irradiated polysiloxane surfaces. J Mater Sci Mater Med. 2003;14:663–70.